PAPER

Multi-round QAOA and advanced mixers on a trapped-ion quantum computer

To cite this article: Yingyue Zhu et al 2023 Quantum Sci. Technol. 8 015007

View the article online for updates and enhancements.

You may also like

- Expectation values from the single-layer quantum approximate optimization algorithm on Ising problems Asier Ozaeta, Wim van Dam and Peter L McMahon
- Hybrid quantum-classical optimization with cardinality constraints and applications to finance Samuel Fernández-Lorenzo, Diego Porras and Juan José García-Ripoll
- To quantum or not to quantum: towards algorithm selection in near-term quantum optimization Charles Moussa, Henri Calandra and Vedran Dunjko



IOP | ebooks™

Bringing together innovative digital publishing with leading authors from the global scientific community.

Start exploring the collection-download the first chapter of every title for free.

Quantum Science and Technology



RECEIVED 20 April 2022

REVISED 3 August 2022

ACCEPTED FOR PUBLICATION 14 September 2022

PUBLISHED

2 November 2022

PAPER

Multi-round QAOA and advanced mixers on a trapped-ion quantum computer

Yingyue Zhu^{1,*}, Zewen Zhang², Bhuvanesh Sundar^{3,4}, Alaina M Green¹, C Huerta Alderete¹, Nhung H Nguyen¹, Kaden R A Hazzard^{2,5} and Norbert M Linke^{1,6}

- Joint Quantum Institute and Department of Physics, University of Maryland, College Park, MD 20740, United States of America
- Department of Physics and Astronomy, Rice University, Houston, TX 77005, United States of America
- JILA, Department of Physics, University of Colorado, Boulder, CO 80309, United States of America
- Center for Theory of Quantum Matter, University of Colorado, Boulder, CO 80309, United States of America
- Rice Center for Quantum Materials, Rice University, Houston, TX 77005, United States of America
- Duke Quantum Center and Department of Physics, Duke University, Durham, NC 27708, United States of America
- Author to whom any correspondence should be addressed.

E-mail: yzhu18@umd.edu

Keywords: QAOA, hybrid quantum algorithm, optimization problems, trapped-ion quantum computing, Grover mixer, fair sampling, graph problems

Abstract

Combinatorial optimization problems on graphs have broad applications in science and engineering. The quantum approximate optimization algorithm (QAOA) is a method to solve these problems on a quantum computer by applying multiple rounds of variational circuits. However, there exist several challenges limiting the application of QAOA to real-world problems. In this paper, we demonstrate on a trapped-ion quantum computer that QAOA results improve with the number of rounds for multiple problems on several arbitrary graphs. We also demonstrate an advanced mixing Hamiltonian that allows sampling of all optimal solutions with predetermined weights. Our results are a step toward applying quantum algorithms to real-world problems.

1. Introduction

Combinatorial optimization problems on graphs are ubiquitous in fields of science and engineering, such as bioinformatics [1, 2], Earth science [3], logistics [4], resource management [5], telecommunications [6], e-commerce [7, 8] and others. Efficient classical algorithms for solving many of these problems are not known, and quantum computers can potentially provide an advantage. The quantum approximate optimization algorithm (QAOA) has been used in several demonstrations to solve combinatorial as well as other types of optimization problems [9-17]. QAOA is a quantum-classical hybrid algorithm that produces high-quality approximate solutions [18]. Even though it does not always guarantee an advantage over classical algorithms, QAOA can achieve a provable quadratic speedup in oracle calls when it is equivalent to Grover's algorithm [19], and numerical evidence shows that it can provide a polynomial speedup in some problems [20]. It has also been argued that even the output distribution from a one-round QAOA circuit is hard to sample classically [21]. QAOA is also able to generate approximate answers with low-depth circuits, which makes it valuable for implementations on near-term quantum devices.

In QAOA, two non-commuting Hamiltonians, the problem-dependent Hamiltonian H_A and the mixing Hamiltonian H_B , are applied repeatedly to a chosen initial state $|\psi_{\text{initial}}\rangle$ in a bang-bang protocol. The final output state is an approximate ground state of H_A as well as a solution to the optimization problem.

$$|\psi_{\text{final}}\rangle = \prod_{i=1}^{p} e^{-iH_{B}\beta_{i}} e^{-iH_{A}\alpha_{i}} |\psi_{\text{initial}}\rangle$$
 (1)

 α_i and β_i are real variational parameters, and p is the number of QAOA rounds. The variational parameters are optimized classically to minimize the expectation value $\langle \psi_{\text{final}} | H_A | \psi_{\text{final}} \rangle$. $|\psi_{\text{initial}} \rangle$ is the ground state of H_B . In standard QAOA, H_B is the n-qubit transverse-field Hamiltonian

$$H_B^{\text{transverse}} = \sum_{i=1}^n \sigma_i^x,\tag{2}$$

where σ_i^x is the Pauli X matrix acting on qubit i.

In theory, QAOA performance improves as p is increased. However, increasing p can degrade the results in practice when the experimental errors introduced by deeper circuits outcompete the theoretical QAOA gain. Additionally, if the connectivity of the graphs does not match the qubit connectivity of the quantum hardware, the overheads required to map these nonnative graphs to the qubits also greatly increase the circuit depth. Moreover, the standard QAOA often provides only a subset of the ground states, while many applications require knowledge about all of them.

The first result of our work is to show that the probability of finding a ground state with standard QAOA increases with p, up to p = 3, on a trapped-ion quantum computer for optimization problems defined on arbitrary graphs. Previous experimental works have demonstrated QAOA results improving with p on hardware-native graphs [9, 10, 14, 15], while real-world graph problems are often hardware-nonnative.

The second result of our work is to demonstrate that employing advanced mixing Hamiltonians in QAOA can allow one to access a broader range of classically hard optimization problems. The recently proposed Grover mixer QAOA (G-QAOA) [22, 23] is capable of generating a superposition of all ground states with probabilities determined by their weights, which are defined in the optimization problem and provided as inputs. This feature is referred to as fair sampling. G-QAOA can be applied to both unweighted and weighted graph problems. The *n*-qubit Grover mixer takes the form

$$H_B^{\text{Grover}} = \prod_{i=1}^n \frac{1 + (1 - 2q)\sigma_i^z + 2\sqrt{q(1 - q)}\sigma_i^x}{2},\tag{3}$$

where q is related to the numerical weight assigned to all qubits, with q=0.5 corresponding to unweighted problems. Other important tasks relying on fair sampling include satisfiability-based membership filters [24–26], proportional model sampling [27], machine learning [28, 29], and sampling the ground states of arbitrary classical spin Hamiltonians [30, 31]. Although in theory G-QAOA fairly samples ground states at any p, the total probability of finding ground states increases with p. While previous works have experimentally demonstrated one round of G-QAOA in Hamiltonian optimization problems on unweighted graphs [32, 33], we apply G-QAOA to both weighted and unweighted graph problems up to p=2 on arbitrary graphs, and quantitatively evaluate the experimental fair sampling results.

The experiments are implemented on a programmable trapped-ion quantum computer, where up to five $^{171}{\rm Yb}^+$ ions in a linear chain are used as qubits. The qubit states $|0\rangle$ and $|1\rangle$ are encoded in the two hyperfine ground states $|F=0,m_F=0\rangle$ and $|F=1,m_F=0\rangle$ in the $^2{\rm S}_{1/2}$ manifold. The qubits are initialized in $|0\rangle$ by optical pumping and read out with state-dependent fluorescence. Quantum controls are implemented by coherently manipulating the qubit states with two counter-propagating Raman beams, one of which is split into individual beams to address each qubit separately (see section 4.2 for more details).

2. Results

2.1. Higher-round QAOA on graph problems

In this section, we focus on finding a maximum cut on the bridge graph and an edge cover on the triangle, paw and square graphs with standard QAOA. All graphs discussed in this section are unweighted. A graph G is defined by a set of vertices $v \in V$, $|V| = N_v$, and a set of edges $e \in E$, $|E| = N_e$. A maximum cut is a partition of all vertices into two complementary sets where the number of edges between them is maximized. An edge cover is a subgraph $G' \subseteq G$ in which every $v \in V$ is connected to at least one edge E' included in G'. A graph can have multiple maximum cuts or edge covers. Although brute force solutions of the maximum cut problem on planar graphs and the edge cover problem can be carried out in polynomial time, the algorithms we employ do not exploit this structure.

Based on the graph problem to be solved, we construct the problem-dependent Hamiltonian H_A such that minimizing H_A gives the solutions of interest. When mapping the graphs onto a quantum computer, a qubit can represent either an edge or a vertex. In Max-Cut problems, the qubits encode the vertices. Each computational basis state represents a partition of V with all vertices corresponding to qubits in state $|0\rangle$ in

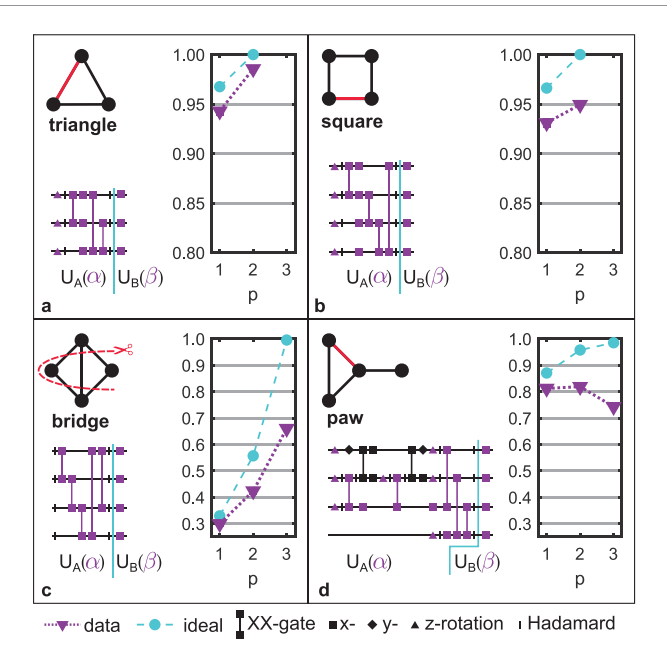


Figure 1. Simulated and experimental results from standard QAOA for the edge cover and Max-Cut problems. The plots give the probability to find a solution on the trapped-ion machine compared to the ideal result for different numbers of QAOA rounds p. The graphs are indicated in the top left corner, i.e. the triangle (a), square (b), bridge (c) and paw graph (d). For edge cover problems (a), (b), (d) the black links show example solutions, for the Max-Cut problem (c) the red line indicates the unique cut. Circuits show one round of the problem unitary $U_A = e^{-iH_A\alpha}$ and the mixer unitary $U_B = e^{-iH_B\beta}$, with purple gates parameterized by α or β . The values of parameters α_i and β_i are listed in section 4.3. All qubits are initialized in the x-basis and measured in the z-basis (not shown). Statistical error bars on the data are calculated from 4000 experimental shots per data point. The error bars are all smaller than 1% in value and smaller than the symbols in the figure. The dashed lines are a guide to the eye.

one set and the rest in the other set. The probability of finding each ground state is the population of the corresponding quantum state in $|\psi_{\text{final}}\rangle$. The problem Hamiltonian H_A for Max-Cut problems is

$$H_A^{\text{maxcut}} = \sum_{(i,j)\in E} \sigma_i^z \sigma_j^z,\tag{4}$$

where σ^z is the Pauli Z operator. If (i, j) is an edge between sets, $\sigma_i^z \sigma_i^z = -1$.

In an edge cover problem, each qubit encodes a unique edge $e \in E$. Therefore, each computational basis state encodes a unique G' where the qubit state $|0\rangle$ ($|1\rangle$) means that the corresponding edge is included (not included) in G'. H_A encoding the edge cover problem is

$$H_A^{\text{ec}} = \sum_{v \in V} \prod_{e \in E(v)} \frac{1 - \sigma_e^z}{2},\tag{5}$$

where E(v) is the set of edges incident on vertex v in G. For a subgraph G', the product term for each v in $H_A^{\rm ec}$ is 0 if there is at least one edge incident on v, otherwise it is 1. Therefore the energy of $H_A^{\rm ec}$ is minimized to 0 if and only if G' is an edge cover.

In the experiment, the system is first prepared in the ground state of H_B in equation (2), $|\psi_{\text{initial}}\rangle = |++\cdots+\rangle$ with $|+\rangle = \frac{1}{\sqrt{2}}(|0\rangle+|1\rangle)$, by applying a Hadamard gate to each qubit. Then the system unitarily evolves under H_A and H_B alternately before being measured in the computational basis.

The results are shown in figure 1 and in table 1 (left column). In the Max-Cut problem on the bridge graph, the probability of finding a *maximum cut* clearly improves with p (figure 1(c)), despite the p-fold increase in the number of gate operations. Similarly, the probabilities of finding one *edge cover* on the triangle and square graph also increase with p (figures 1(a) and (b)).

However, on the paw graph, the probability of finding an *edge cover* only improves marginally for p=2 and drops for p=3 (figure 1(d)). In this problem, the implementation of $H_A^{\rm ec}$ requires seven two-qubit entangling gates, the most among all four problems, and the additional gate error outweighs the theoretical gain with increasing p. The question then arises whether there are alternatives to increasing p that will improve the solution probability. One such idea is to use more sophisticated mixers, an example of which is the Grover-mixer given in equation (3). While, as we will see, this does not increase the solution probability

Table 1. Simulated and experimental probabilities of finding a ground state for different p by standard QAOA (left half) and G-QAOA (right half) for the edge cover (triangle, paw, and square graph) and Max-Cut problems (bridge graph). The errors are the statistical 68.3% confidence interval.

Standard QAOA				G-QAOA				
Graph		p = 1	p = 2	p = 3	Graph		p = 1	p = 2
Triangle	Sim Exp	0.968 0.943(2)	1 0.986(1)		Triangle	Sim Exp	0.781 0.739(2)	0.999 0.751(2)
Square	Sim Exp	0.966 0.931(1)	1 0.949(1)		Square	Sim Exp	0.770 0.668(1)	0.801 0.692(1)
Paw	Sim Exp	0.871 0.812(2)	0.958 0.819(1)	0.985 0.743(2)	Paw	Sim Exp	0.645 0.548(2)	0.867 0.551(2)
Bridge	Sim Exp	0.330 0.300(3)	0.557 0.424(4)	0.996 0.660(4)	Paw (weighted)	Sim Exp	0.105 0.235(1)	0.835 0.421(1)
					Square (weighted)	Sim Exp	0.310 0.255(1)	0.758 0.497(1)

for a fixed gate depth, it does enable the solution of a new class of graph optimization problem—sampling problems.

2.2. Sampling with G-QAOA on unweighted graphs

All four unweighted graph problems studied in section 2.1 have more than one solution, but we observe that the standard QAOA favors only one. G-QAOA samples all ground states with equal probability at any p on unweighted graphs. In this section, the goal is to find all solutions for the three edge cover problems studied in section 2.1 by using G-QAOA. H_A^{ec} is given in equation (5). But now H_B is the Grover mixer for unweighted graphs given in equation (3) with q = 0.5. Circuits for implementing the Grover mixer can be found in figures 4 and 5 in section 4.3.

Figure 2 shows the individual probabilities of finding each ground state for each problem, and table 1 gives the total probability of finding all ground states. The blue bars in figure 2 demonstrate our claim that standard QAOA favors one solution more than others, while the purple bars show that G-QAOA does not. In the G-QAOA result for the edge cover problem on the triangle graph at p=1, the experiment closely approximates the simulation. Furthermore, we see a small improvement in the total ground state probabilities at p=2 compared with p=1 for all three graphs despite the deeper circuits at higher p.

Fairness describes how well the experimentally sampled distribution represents the ideal distribution. The fair sampling of ground states with equal probabilities provides a convenient method to enumerate all ground states of a problem. One measure of the efficiency of the enumeration is the average number of experimental shots required to observe each ground state at least once. To estimate this, we sample the states from the experimentally measured distributions on a classical computer. For each experimental distribution, we record the number of random draws required to observe any $N_{\rm g}$ different ground states at least once, varying $N_{\rm g}$ from 2 to the total number of ground states. For each $N_{\rm g}$ we repeat the procedure for 100 000 times to determine the average number of draws and the uncertainty.

Table 2 shows that, at p=1, G-QAOA and QAOA perform similarly at enumerating ground states, with QAOA being marginally more efficient in most cases. The only exception is the paw graph problem for $N_{\rm g}=5$, where the ground state with the smallest probability found by QAOA (the fourth ground state from the left, see figure 2) has considerably lower probability in both simulation and experiment than the ground state with the smallest probability found by G-QAOA. Since the efficiency of enumerating by sampling is limited by the ground states with the lowest probability, G-QAOA shows an advantage in this case. QAOA at p=2 suppresses some ground states more strongly than at p=1, and therefore has the worst results. G-QAOA at p=2 shows results similar to G-QAOA at p=1, with slight improvement seen in a few cases. This differs from the ideal prediction that the number of draws required should decrease from p=1 to p=2 for G-QAOA since the total probability of ground states grows. However, in experiment the total probabilities do not increase significantly due to decoherence (see table 1). For the same reason, we see that most often QAOA at p=1 requires the least number of draws to find $N_{\rm g}$ ground states, while theory predicts that G-QAOA at p=2 should have an advantage in most cases, especially when $N_{\rm g}$ is close to the total number of ground states. Nevertheless, G-QAOA at p=1 and p=2 still require fewer samples than random guessing to obtain all ground states.

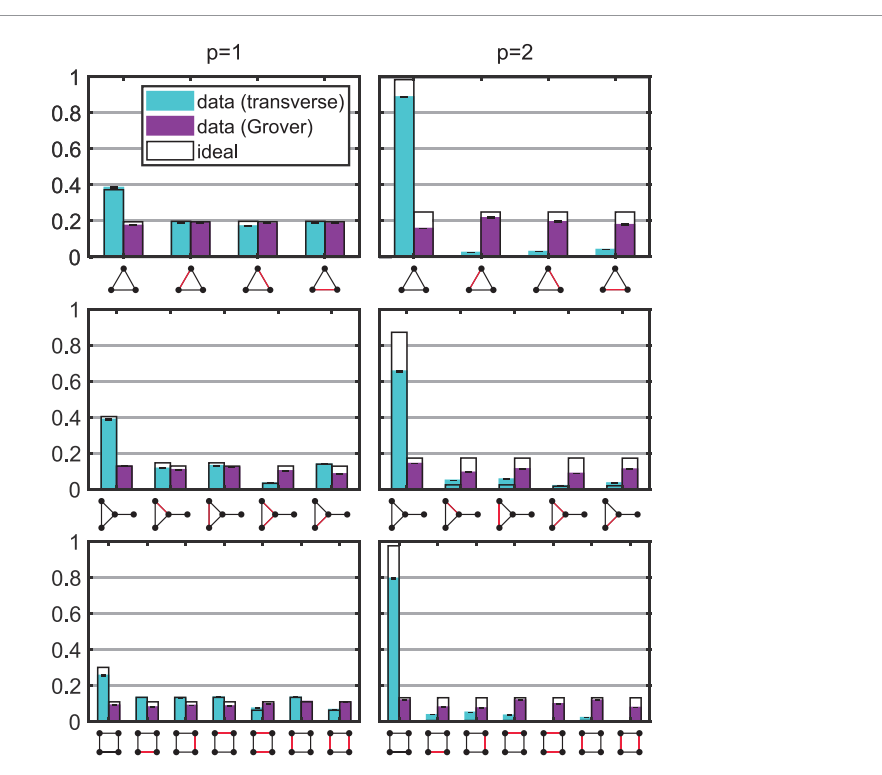


Figure 2. Simulated and experimental probabilities of finding each ground state by standard QAOA and G-QAOA for the edge cover problems on the triangle, paw, and square graph. Each plot compares the individual probabilities of finding each ground state at the same *p* for the same problem between standard QAOA and G-QAOA. Different *edge covers* are illustrated at the bottom of each plot on the horizontal axis, with edges included in each specific *edge cover* colored in black and edges not included colored in red. Simulated probabilities are delineated in contour with solid black lines, overlapping with corresponding experimental data plotted with colored bar without any outline. Error bars are calculated from 4000 experimental shots and are shown as short black dashes.

Table 2. Number of draws required to see $N_{\rm g}$ ground states on unweighted graphs. Average and error bars are calculated from 100 000 independent trials. All error bars less than 0.01 are not included in the table. In comparison, if this similar counting test is done on random guessing (p=0), it will take 16.64(3), 36.58(6) and 41.40(4) of draws in these three graphs to get all ground states.

		$(N_{ m g})$	2	3	4	5	6	7
Triangle	p = 1	QAOA G-QAOA	2.58 3.15	5.00 5.87	10.16 11.28			
	p = 2	QAOA G-QAOA	10.43 3.11	26.48 5.82	60.50(1) 11.30(2)			
Paw	p = 1	QAOA G-QAOA	3.13 4.12	6.15 7.19	11.65 11.91	33.34 21.54		
	p = 2	QAOA G-QAOA	6.44 4.09	14.93 7.20(1)	29.20(6) 11.93	66.0(1) 21.61(3)		
Square	p = 1	QAOA G-QAOA	2.53 3.16	4.28 5.22	6.55 7.84	9.78 11.4(1)	15.05 16.82	25.09 28.12
	p=2	QAOA G-QAOA	6.64 3.25	15.33 5.36	28.41 7.99	53.7(1) 11.56	171.1(5) 16.87	493(1) 27.69

2.3. Fair-sampling with G-QAOA on weighted graphs

In this section, we solve the edge cover problem when a numerical weight (1-q)>0 with $q\neq 0.5$ is assigned to all edges on the paw and square graph. The weight of each subgraph G' is defined as $P_{G'}=(1-q)^{n'}q^{n-n'}$, where n' is the number of edges included in G'. G-QAOA samples all ground states, with squared amplitudes proportional to these weights.

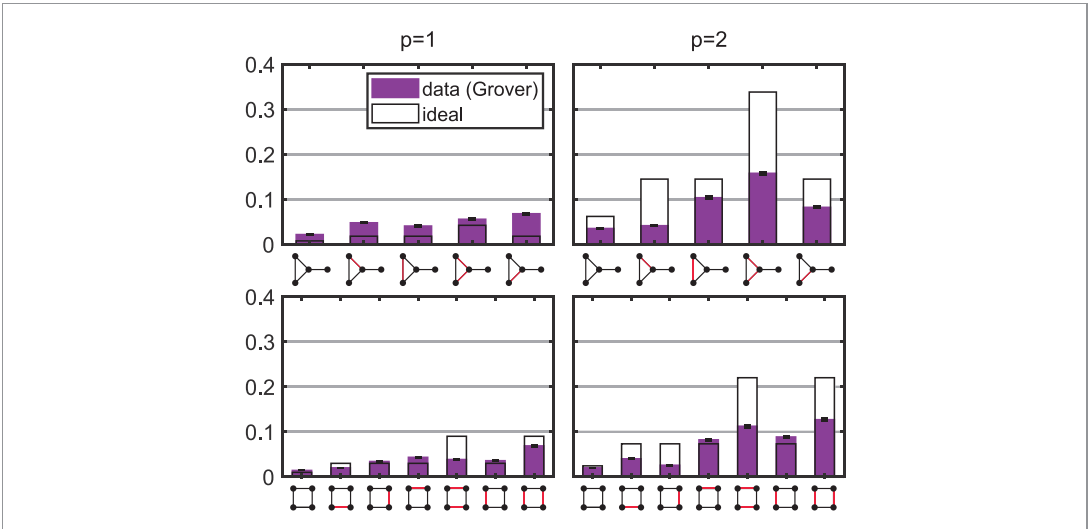


Figure 3. Simulated and experimental results from G-QAOA for the edge cover problem on the weighted paw (top) and square (bottom) graph. Error bars shown as short black dashes are calculated from 4000 experimental shots.

 H_A^{ec} is given in equation (5) as in the previous two sections. H_B is the Grover mixer given in equation (3). The initial state is prepared by applying

$$U = e^{-i\sigma^y \sin^{-1}\sqrt{q}} \tag{6}$$

to each qubit in $|0\rangle$. Figure 3 shows the G-QAOA results on a paw graph with q = 0.7 and a square graph with q = 0.75, and compares them to the ideal population distributions.

To allow direct fairness comparisons between results for problems with different numbers of ground states and different sample sizes N on weighted graphs, we need a metric that is insensitive to these problem specifics. Fairness of the sampling result can be quantified as the discrepancy between the ideal ground state distribution Q_1 and the experimentally measured ground state distribution Q_1 , which is obtained by post-selecting out all ground states from 4000 experimental shots. The first method we adopt is the 'shots to reject' method, proposed in reference [32], which is constructed based on the chi-squared (χ^2) test. By re-sampling from Q_1 , the goal is to compute the number of samples, N^* , needed to reject the null hypothesis H_0 at a selected significance level. Here, H_0 is that Q_1 is sampled from Q_2 . The more the experimental data Q_1 deviates from the ideal distribution Q_2 , the smaller N^* will be. To find N^* , we follow the protocol described in section 4.1.

Table 3 shows the results for N^* from the experimental data with synthetic data for comparison, where synthetic data are random samples drawn from Q_2 on a classical computer. Some ground states on the weighted graphs have very small expected populations, causing H_0 to be more easily rejected in the χ^2 test, which contributes to the sampling results being overall less fair on the weighted than on the unweighted graphs for both experimental and synthetic data. We see a clear improvement in the fairness going from p=1 to p=2 in both weighted problems. This is due to G-QAOA boosting the probabilities of most of the ground states, including the least likely one, in each problem (see figure 3 and table 1). When generating the synthetic data with a fixed number of draws from the entire population, the ground state counts are larger for p=2 than p=1, leading to different 'shots to reject' results.

An alternative way to characterize the differences between probability distributions is the Kullback–Leibler (KL) divergence. The results for the KL divergence analysis are presented in table 4 in section 4.1. All trends are consistent with that seen in the 'shots to reject' analysis.

3. Outlook

In this work, we experimentally demonstrated that the standard QAOA results improve with increasing p up to p=3 in optimization problems on arbitrary graphs, and show fair sampling results of G-QAOA up to p=2 on both unweighted and weighted graphs on a trapped-ion quantum computer. To push beyond these small demonstration problems, advances in fidelity and system size of the quantum hardware are crucial. Additionally, future studies on large-scale arbitrary graphs will challenge the connectivity of all hardware platforms, which highlights the importance of efficiently matching graphs and architectures.

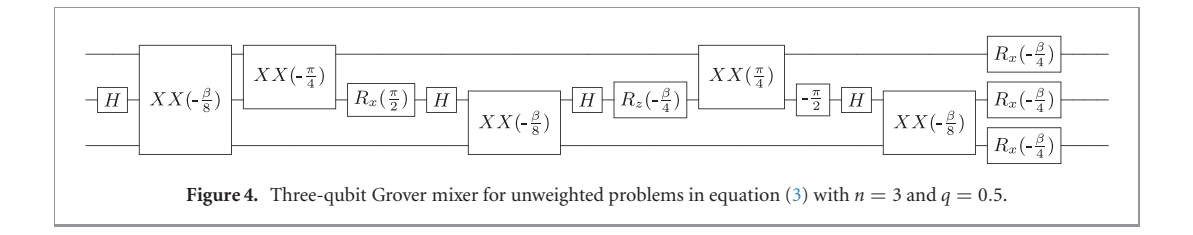
Table 3. Number of shots to reject the fair sampling hypothesis by re-sampling from the experimental data and the synthetic data. The synthetic data is randomly drawn from the ideal distributions. Averages and error bars are calculated by repeating the 'shots to reject' test 10 times.

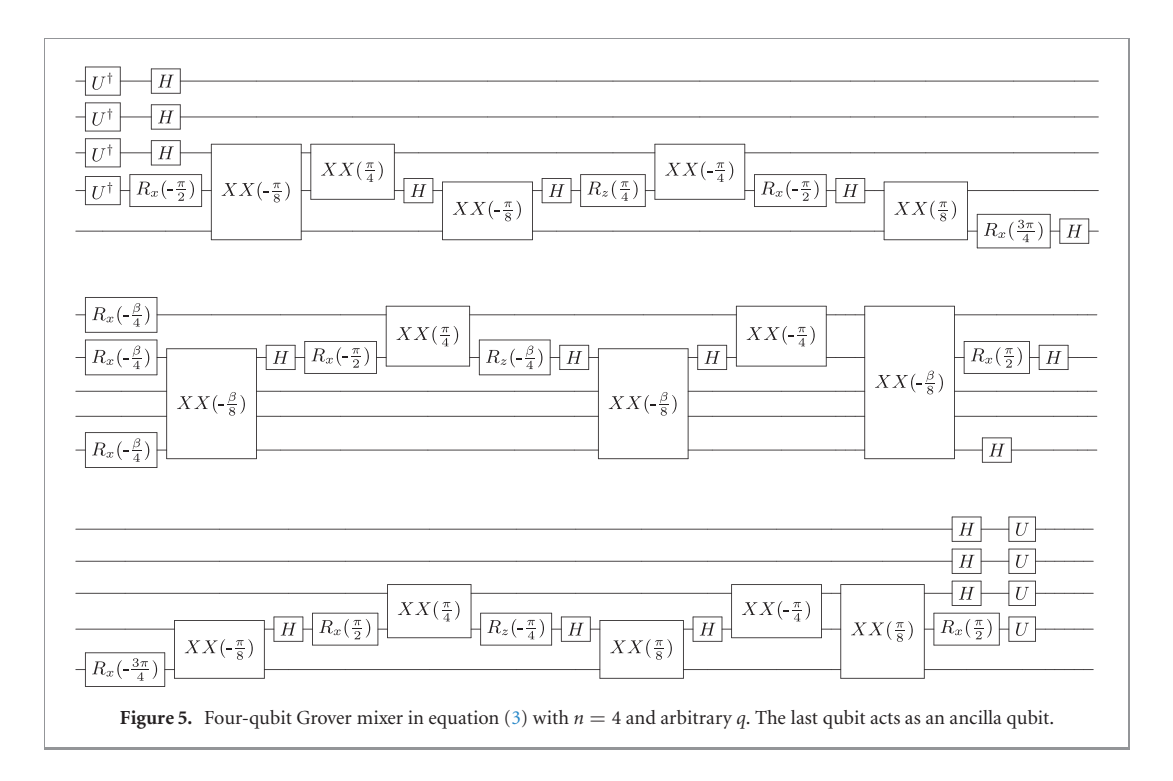
	(a) Experi	mental data	
		p = 1	p = 2
Unweighted	Triangle Paw Square	5754(32) 328(4) 602(13)	406(8) 208(4) 192(4)
Weighted	Paw Square	38(1) 35(1)	90(1) 45(1)
	(b) Synt	hetic data	
		p = 1	p = 2
Unweighted	Inweighted Triangle Paw Square		4337(943) 4044(702) 2318(247)
Weighted	Paw Square	297(74) 674(82)	1958(675) 1370(270)

Table 4. KL divergence between the simulation and experimental data, and synthetic data. The error bar on each experimental result is calculated by resampling from the experimental distribution 300 times, while for each synthetic result it comes from 300 sets of synthetic data generated for each problem.

	(a) Experin	nental data	
		p = 1	p = 2
Unweighted	Triangle	0.0007(4)	0.007(2)
_	Paw	0.015(2)	0.016(2)
	Square	0.007(1)	0.020(2)
Weighted	Paw	0.079(8)	0.037(4)
	Square	0.089(9)	0.074(6)
	(b) Synth	etic data	
		p = 1	p = 2
Unweighted	Triangle	0.0004(2)	0.0003(1)
_	Paw	0.0006(3)	0.0005(2)
	Square	0.0008(3)	0.0007(3)
Weighted	Paw	0.004(2)	0.0005(2)
	Square	0.0021(8)	0.0009(3)

Although G-QAOA does not show an advantage at enumerating the ground states over standard QAOA or when going to higher p on unweighted graphs due to experimental noise, we do observe that the total probabilities of ground states grow with increasing p in all cases. We also observe the fairness of sampling improves with increasing p in the two weighted problems. Future experiments could look at the relative advantage provided by more advanced mixers, such as the QED-inspired mixer designed for constrained flow problems [34], follow general guidelines to engineer mixers that ensure solutions satisfy desired constraints [35] or symmetries [36], and study circuits which preserve specific physical symmetries in optimization problems in fermionic systems [37].





4. The methods

4.1. Statistical tests

The 'shots to reject' test used in section 2.3 is based on the one-tailed χ^2 test. To find N^* , we implement the following steps: (1) randomly draw 1000 sets of samples of size M (starting from M=2) from Q_1 , perform a χ^2 test between each sampled distribution and Q_2 , and record the 1000 p-values from the tests, (2) compare the median of the p-values with the preset significance level, which is chosen to be 0.05 here, (3) if the median of the p-values exceeds the threshold, set M:=2M and repeat steps 1 to 2; otherwise, if the median p-value is smaller than the threshold, H_0 is rejected, then a bisection method is used to locate the exact N^* between M and M/2.

The KL divergence used in section 2.3 is defined as

$$D_{\mathrm{KL}}(Q_1 || Q_2) = \sum_{x \in X} Q_1(x) \frac{Q_1(x)}{Q_2(x)},\tag{7}$$

where X is the sample space. It can be intuitively understood as the information loss when we model Q_2 by Q_1 , providing the distance between the two distributions. The results for this analysis in section 2.3 are presented in table 4.

4.2. Experimental setup

The experiment is implemented on a programmable universal trapped-ion quantum computer with up to nine qubits and individual ion addressability. The native gate set includes single-qubit rotations around an arbitrary axis \vec{n} in the x-y plane of the Bloch sphere by angle θ , $R(\hat{n},\theta) = \mathrm{e}^{-\mathrm{i}\vec{\sigma}\cdot\vec{n}\,\theta/2}$, rotations around the z axis $R_z(\theta) = \mathrm{e}^{-\mathrm{i}\sigma_z\theta/2}$, and the two-qubit interaction $XX = \mathrm{e}^{\mathrm{i}\theta\sigma_x^i\sigma_x^j}$ between any pair of qubits for arbitrary θ . The $R(\hat{n},\theta)$ are realized via resonant Raman transitions with duration proportional to θ . The $R_z(\theta) = \mathrm{e}^{-\mathrm{i}\sigma_z\theta/2}$ gates are classical phase advances in the laser beam controllers. The two-qubit entangling

Table 5. Standard QAOA and G-QAOA parameters.

(a) Standard QAOA parameters co	rresponding to results in figure 1 ar	nd table 1 (left)
	p = 1	p = 2	p = 3
Triangle	$\alpha = -0.95, \beta = 1.00$	$\alpha_1 = -0.83, \beta_1 = 3.14$ $\alpha_2 = 0.85, \beta_2 = -1.66$	
Square	$\alpha = -0.87, \beta = -2.60$	$\alpha_1 = 0.80, \beta_1 = -1.58$ $\alpha_2 = -0.82, \beta_2 = -2.28$	
Paw	$\alpha = 1.04, \beta = -0.61$	$lpha_1 = 0.62, eta_1 = 0.75 \ lpha_2 = 0.88, eta_2 = -1.04$	$\alpha_1 = 0.5, \beta_1 = 1.6$ $\alpha_2 = -0.5, \beta_2 = 0.5$ $\alpha_3 = -0.5, \beta_3 = 0.3$
Bridge	$\alpha=0.29,\beta=0.31$	$\alpha_1 = -0.55, \beta_1 = 0.42$ $\alpha_2 = -2.95, \beta_2 = 0.87$	$\alpha_1 = -2.09, \beta_1 = 0.43$ $\alpha_2 = -2.17, \beta_2 = 1.28$ $\alpha_3 = -1.02, \beta_3 = 2.3$
(b) G-QAC	A parameters for unweighted prol	blems corresponding to results in fi	gure 2 and table 1 (right)
	p = 1	p = 2	
Triangle	$\alpha = 2.48, \beta = 1.37$	$\alpha_1 = 0.69, \beta_1 = 1.32$ $\alpha_2 = 1.22, \beta_2 = 0.92$	
Square	$\alpha=0.65,\beta=1.46$	$\alpha_1 = 0.48, \beta_1 = 1.52$ $\alpha_2 = 0.91, \beta_2 = 0.92$	
Paw	$\alpha = 0.79, \beta = 1.60$	$ \alpha_1 = 0.56, \beta_1 = 1.47 $ $ \alpha_2 = 0.98, \beta_2 = 1.17 $	
	(c) G-QAOA parameters for weigh	nted problems corresponding to res	ults in figure 3
	p = 1	p = 2	
Square	$\alpha = 2.67, \beta = -2.30$	$\alpha_1 = 0.68, \beta_1 = 2.20$ $\alpha_2 = 1.05, \beta_2 = 1.90$	
Paw	$\alpha = -2.85, \beta = 2.81$	$ \alpha_1 = 2.05, \beta_1 = 2.80 $ $ \alpha_2 = 1.98, \beta_2 = 2.90 $	

gates are implemented using the Mølmer–Sørensen scheme [38, 39], where the qubit spin states and the collective motional modes of the ion chain are coupled and decoupled via amplitude-modulated laser pulses [41]. The typical single- and two-qubit gate times are 10 and 200 ms. The longest circuit implemented in this work, consisting of 44 two-qubit gates and about 150 single-qubit gates, has a total run time of a few milliseconds. In contrast, the qubit coherence time is on the order of 1 s. The typical single- and two-qubit gate fidelities are 99.5(2)% and 98%–99% respectively. In this setup, two-qubit gate infidelity is the main source of experimental error. More details about the experimental setup are described in reference [42].

4.3. Circuits and parameters

The circuit in figure 4 shows the three-qubit Grover mixer for unweighted problems used in the edge cover problem on the unweighted triangle graph. Figure 5 shows the four-qubit Grover mixer. Variational parameters α and β for each problem are listed in table 5. These optimal parameter sets are derived from a noise-free theory using exact numerics. For the edge-cover problems, we perform a global grid search for the parameters starting with a resolution of 0.1 and keep refining the best results via a local grid search with successively finer resolutions until we reach the desired resolution, which is set to 0.01 for most problems and 0.1 for p=3 paw graph with the simple mixer. For the Max-Cut problem, we use the *FindMinimum* function in *Mathematica* [40] and pick the best result out of at least 10 independent searches.

Acknowledgments

KRAH and NML acknowledge funding by the Office of Naval Research (N00014-20-1-2695). This research was supported in part by the NSF (PHY-1430094, PHY-1848304, CMMI-2037545) and the Robert A Welch

Foundation (C-1872). AMG is supported by a Joint Quantum Institute Postdoctoral Fellowship. NML acknowledges support by the Maryland-Army-Research-Lab Quantum Partnership (W911NF1920181).

Data availability statement

The data that support the findings of this study are available from the corresponding author upon request.

Conflict of interest

The authors do not declare any conflicts of interest.

Author contributions

BS, ZZ and KRH formulated the theory. YZ, ZZ, BS, NML and KRH designed the experiment. YZ, AMG, CHA, and NHN implemented the experiment. ZZ and YZ performed the data analyses. This manuscript is written by YZ, and all other authors contributed to editing the manuscript.

ORCID iDs

```
Yingyue Zhu https://orcid.org/0000-0002-9891-231X

Zewen Zhang https://orcid.org/0000-0003-2258-613X

Bhuvanesh Sundar https://orcid.org/0000-0002-8867-360X

Alaina M Green https://orcid.org/0000-0003-3365-4433

C Huerta Alderete https://orcid.org/0000-0003-3673-9985

Nhung H Nguyen https://orcid.org/0000-0002-0462-9258

Kaden R A Hazzard https://orcid.org/0000-0003-2894-7274
```

References

- [1] Duvenaud D K, Maclaurin D, Iparraguirre J, Bombarell R, Hirzel T, Aspuru-Guzik A and Adams R P 2015 Convolutional networks on graphs for learning molecular fingerprints (arXiv:1509.09292v2 [cs.LG])
- [2] Yue X et al 2020 Graph embedding on biomedical networks: methods, applications and evaluations Bioinformatics 36 1241
- [3] Hobé A, Vogler D, Seybold M P, Ebigbo A, Settgast R R and Saar M O 2018 Estimating fluid flow rates through fracture networks using combinatorial optimization *Adv. Water Resour.* 122 85
- [4] Sbihi A and Eglese R W 2007 Combinatorial optimization and green logistics 4OR 5 99
- [5] Eskandarpour M, Dejax P, Miemczyk J and Péton O 2015 Sustainable supply chain network design: an optimization-oriented review Omega 54 11
- [6] Resende M G C 2003 Combinatorial optimization in telecommunications *Optimization and Industry: New Frontiers (Applied Optimization* vol 78) ed P M Pardalos and V Korotkikh (Boston, MA: Springer)
- [7] Fan W, Ma Y, Li Q, He Y, Zhao E, Tang J and Yin D 2019 Graph neural networks for social recommendation (arXiv:1902.07243 [cs.IR])
- [8] Zhang F, Yuan N J, Lian D, Xie X and Ma W-Y 2016 Collaborative knowledge base embedding for recommender systems *Proc. ACM SIGKDD Int. Conf. Knowl.*
- [9] Bengtsson A et al 2020 Improved success probability with greater circuit depth for the quantum approximate optimization algorithm Phys. Rev. Appl. 14 034010
- [10] Harrigan M P et al 2021 Quantum approximate optimization of non-planar graph problems on a planar superconducting
- [11] Qiang X et al 2018 Large-scale silicon quantum photonics implementing arbitrary two-qubit processing Nat. Photon. 12 534
- [12] Willsch M, Willsch D, Jin F, De Raedt H and Michielsen K 2020 Benchmarking the quantum approximate optimization algorithm Quantum Inf. Process. 19 197
- [13] Abrams D M, Didier N, Johnson B R, de Silva M P and Ryan C A 2020 Implementation of XY entangling gates with a single calibrated pulse Nat. Electron. 3 744
- [14] Lao L and Browne D 2021 2qan: a quantum compiler for two-local qubit Hamiltonian simulation algorithms (arXiv:2108.02099 [quant-ph])
- [15] Lacroix N et al 2020 Improving the performance of deep quantum optimization algorithms with continuous gate sets PRX Quantum 1 110304
- [16] Pagano G et al 2020 Quantum approximate optimization of the long-range Ising model with a trapped-ion quantum simulator Proc. Natl Acad. Sci. 117 25396
- [17] Otterbach J S et al 2017 Unsupervised machine learning on a hybrid quantum computer (arXiv:1712.05771 [quant-ph])
- [18] Farhi E, Goldstone J and Gutmann S 2014 A quantum approximate optimization algorithm (arXiv:1411.4028 [quant-ph])
- [19] Niu M Y, Lu S and Chuang I L 2019 Optimizing QAOA: success probability and runtime dependence on circuit depth (arXiv:1905.12134 [quant-ph])
- [20] Díez-Valle P, Porras D and García-Ripoll J J 2022 QAOA pseudo-Boltzmann states (arXiv:2201.03358 [quant-ph])

- [21] Farhi E and Harrow A W 2019 Quantum supremacy through the quantum approximate optimization algorithm (arXiv:1602.07674 [quant-ph])
- [22] Sundar B, Paredes R, Damanik D T, Dueñas-Osorio L and Hazzard K R A 2019 A quantum algorithm to count weighted ground states of classical spin Hamiltonians (arXiv:1908.01745 [quant-ph])
- [23] Bärtschi A and Eidenbenz S 2020 Grover mixers for QAOA: shifting complexity from mixer design to state preparation 2020 IEEE Int. Conf. on Quantum Computing and Engineering (QCE) pp 72–82
- [24] Weaver S, Ray K J, Marek V W, Mayer A J and Walker A 2014 Satisfiability-based set membership filters J. Satisfiability 8 129
- [25] Douglass A, King A D and Raymond J 2015 Constructing SAT filters with a quantum annealer Theory and Applications of Satisfiability Testing — SAT 2015 ed M Heule and S Weaver (Cham: Springer) pp 104–20
- [26] Azinović M, Herr D, Heim B, Brown E and Troyer M 2017 Assessment of quantum annealing for the construction of satisfiability filters *SciPost. Phys.* 2 013
- [27] Biere A et al 2009 Handbook of Satisfiability ed A Biere, M Heule, H v Maaren and T Walsch (Frontiers in Artificial Intelligence and Applications) (NLD: IOS Press)
- [28] Hinton G E 2002 Training products of experts by minimizing contrastive divergence Neural Comput. 14 1771
- [29] Eslami S M A, Heess N and Winn J 2012 The shape Boltzmann machine: a strong model of object shape 2012 IEEE Conf. on Computer Vision and Pattern Recognition pp 406–13
- [30] Gomes C P, Sabharwal A and Selman B 2006 Model counting: a new strategy for obtaining good bounds Proc. of the 21st National Conf. on Artificial Intelligence—Vol 1, AAAI'06 (AAAI Press) pp 54–61
- [31] Roth D 1996 On the hardness of approximate reasoning Artif. Intell. 82 273
- [32] Golden J, Bärtschi A, O'Malley D and Eidenbenz S 2021 QAOA-based fair sampling on NISQ devices (arXiv:2101.03258 [quant-ph])
- [33] Pelofske E, Golden J, Bärtschi A, O'Malley D and Eidenbenz S 2021 Sampling on NISQ devices: 'who's the fairest one of all?' (arXiv:2107.06468 [quant-ph])
- [34] Zhang Y, Zhang R and Potter A C 2021 QED driven QAOA for network-flow optimization Quantum 5 510
- [35] Hen I and Sarandy M S 2016 Driver Hamiltonians for constrained optimization in quantum annealing Phys. Rev. A 93 062312
- [36] Selvarajan R, Sajjan M and Kais S 2021 Variational quantum circuits to prepare low energy symmetry states (arXiv:2112.12857)
- [37] Gard B T, Zhu L, Barron G S, Mayhall N J, Economou S E and Barnes E 2020 Efficient symmetry-preserving state preparation circuits for the variational quantum eigensolver algorithm NPJ Quantum Inf. 6 10
- [38] Sørensen A and Mølmer K 1999 Quantum computation with ions in thermal motion Phys. Rev. Lett. 82 1971
- [39] Solano E, de Matos Filho R L and Zagury N 1999 Deterministic Bell states and measurement of the motional state of two trapped ions Phys. Rev. A 59 R2539
- [40] W. R. Inc. 2022 Mathematica, Version 13.1 (Champaign, IL)
- [41] Choi T, Debnath S, Manning T A, Figgatt C, Gong Z-X, Duan L-M and Monroe C 2014 Optimal quantum control of multimode couplings between trapped ion qubits for scalable entanglement Phys. Rev. Lett. 112 190502
- [42] Debnath S, Linke N M, Figgatt C, Landsman K A, Wright K and Monroe C 2016 Demonstration of a small programmable quantum computer with atomic qubits *Nature* 536 63